The Journal of Chemical Physics

Efficiency of rovibrational cooling of HeH^+ by collisions with He: Cross sections and rate coefficients from quantum dynamics

Cite as: J. Chem. Phys. **155**, 154301 (2021); https://doi.org/10.1063/5.0062147
Submitted: 02 July 2021 • Accepted: 28 September 2021 • Published Online: 15 October 2021

F. A. Gianturco, K. Giri, L. González-Sánchez, et al.

View Online Export Citation CrossMark

ARTICLES YOU MAY BE INTERESTED IN

Solving the Schrödinger equation using program synthesis
The Journal of Chemical Physics **155**, 154102 (2021); https://doi.org/10.1063/5.0062497

What the foundations of quantum computer science teach us about chemistry
The Journal of Chemical Physics **155**, 150901 (2021); https://doi.org/10.1063/5.0060367

Multi-configuration electron–nuclear dynamics: An open-shell approach
The Journal of Chemical Physics **155**, 154103 (2021); https://doi.org/10.1063/5.0063478

The Journal of Chemical Physics SPECIAL TOPIC: Low-Dimensional Materials for Quantum Information Science Submit Today!

AIP Publishing

© 2021 Author(s).

The Journal of Chemical Physics ARTICLE scitation.org/journal/jcp

Efficiency of rovibrational cooling of HeH^+ by collisions with He: Cross sections and rate coefficients from quantum dynamics

Cite as: J. Chem. Phys. 155, 154301 (2021); doi: 10.1063/5.0062147
Submitted: 2 July 2021 • Accepted: 28 September 2021 •
Published Online: 15 October 2021

View Online Export Citation CrossMark

F. A. Gianturco,[1,a] K. Giri,[2] L. González-Sánchez,[3] E. Yurtsever,[4] N. Sathyamurthy,[5] and R. Wester[1]

AFFILIATIONS

[1] Institut für Ionenphysik und Angewandte Physik, Universität Innsbruck, Technikerstr. 25, A-6020 Innsbruck, Austria
[2] Department of Computational Sciences, Central University of Punjab, Bathinda 151001, India
[3] Departamento de Química Física, University of Salamanca, Plaza de los Caídos sn, 37008 Salamanca, Spain
[4] Department of Chemistry, Koc University, Rumelifeneriyolu, Sariyer, TR 34450 Istanbul, Turkey
[5] Indian Institute of Science Education and Research Mohali, Manauli, SAS Nagar 140306, India

[a] **Author to whom correspondence should be addressed:** francesco.gianturco@uibk.ac.at

ABSTRACT

By extending an earlier study [Gianturco *et al.*, J. Chem. Phys. **154**, 054311 (2021)] on the purely rotational excitation of HeH^+ by He atoms, we report in this paper integral cross sections and rate coefficients for rovibrational excitation and de-excitation processes in HeH^+ due to collisions with He. The data were obtained using a new *ab initio* potential energy surface that includes the vibrational degree of freedom. The results are compared with those computed using the earlier potential energy surface by Panda and Sathyamurthy [J. Phys. Chem. A **107**, 7125 (2003)] that additionally accounts for the proton-exchange reaction between HeH^+ and He. It is shown that the exchange channel contributes nearly as much as the inelastic channel to the vibrational excitation and de-excitation processes and that the total rate constants pertaining to the purely inelastic processes are largely of the same magnitude as those obtained when both inelastic and reactive channels are included in the dynamics. The inelastic rovibrational rate coefficients involving this astrophysical cation are also found to be much larger than those obtained for anions present in similar interstellar environments.

Published under an exclusive license by AIP Publishing. https://doi.org/10.1063/5.0062147

I. INTRODUCTION

The first chemical bond formed between He and H^+ in the early universe is believed to have occurred through radiative association[1,2] (RA) processes,

$$He + H^+ \longrightarrow HeH^+ + h\nu. \quad (1)$$

Although HeH^+ was detected in a mass spectrometer in the laboratory as early as 1925 by Hogness and Lunn,[3] it was suggested as a potential molecular species to be observed in the interstellar medium (ISM) only in 1949 by Wildt[4] and later on by Dabrowski and Herzberg.[5] However, it eluded actual sighting under ISM conditions until rather recently. The first observation of emission from the first excited rotational state ($j = 1$) to the ground rotational state ($j = 0$) in the ground vibrational state ($v = 0$) of HeH^+ at 149.137 μm from planetary nebula (PN) NGC 7027 was reported by Güsten *et al.*[6] This detection was followed by the observation of the infrared emission from $v = 1$ to $v' = 0$ states of HeH^+ at 3.516 29 and 3.607 76 μm as P(1) and P(2) lines, respectively, by Neufeld *et al.*[7] This sighting provided a clear indication of the $v = 1$ state of this cation being populated under those PN conditions.

Our best current understanding[8] is that HeH^+ is formed in PN prevalently through the RA pathway reported by the following equation:

$$He^+ + H \longrightarrow HeH^+ + h\nu. \quad (2)$$

This choice, in contrast with the option provided by Eq. (1) for processes occurring under early universe conditions, stems from the fact that the models of early universe compositions suggest that neutral He is being formed before neutral H so that reactions would be

Published under an exclusive license by AIP Publishing

possible with the protons present in that environment.[1] On the other hand, the different conditions in the planetary nebulae would have both H and He^+ present in the PN so that reaction (2) becomes an important path to the formation of the title cation.[8]

When investigating the efficiency of excitation and de-excitation of different rovibrational states of HeH^+ in its ground electronic state, possible collision partners in the ISM and circumstellar conditions are provided by the most abundant species present there and given as follows: *e*, H, He, and H_2. Electrons have been found to be much more effective than H/He atoms in causing rotational excitations by collisions.[9–12] For example, in the case of the excitation of HeH^+ as a rigid rotor (RR) from its $j = 0$ to its $j' = 1$ states by electron impact, the rate coefficient (k) was found to be of the order of 10^{-6} cm^3 $molecule^{-1}$ s^{-1} in the temperature range of 100–500 K. On the other hand, when H/He are taken as the collision partners, the k value for the same process in the same temperature range is only of the order of 10^{-10} cm^3 $molecule^{-1}$ s^{-1} (see Fig. 9 of Ref. 12). One should also be reminded here that the densities of the relevant species in the PN environments are different in value so that changes in their estimates obviously modify the outcomes of kinetic evolution models.

We have already shown recently[12] that He is as effective as, if not more effective than, the neutral H atoms in causing rotational excitation in HeH^+. In that study, HeH^+ was treated as a rigid rotor (RR) using a newly computed *ab initio* potential energy surface (labeled RR-PES) or by freezing the vibrational degree of freedom for HeH^+ in its $v = 0$ state and then using an earlier three-dimensional (3D) *ab initio* PES published by Panda and Sathyamurthy.[13] The latter was labeled PS-PES in that work. There is also another *ab initio* PES published a while ago by Liang *et al.*,[14] and that was found to be essentially identical to the PS-PES of Panda and Sathyamurthy[13] in all aspects. In fact, the main dynamical outcomes were comparable in magnitude when obtained using either of those potential energy surfaces.[15–17] This was the reason why our earlier dynamical investigations of the rotational excitation/de-excitation dynamics in HeH^+ were restricted to the use of the PS-PES and the more recent RR-PES of Gianturco *et al.*[12]

It is also important to point out at this stage of our discussion that in the PS-PES, there exists a deep potential well (4600 cm^{-1}) corresponding to the linear $[HeHHe]^+$ complex. Panda and Sathyamurthy[13] computed the bound and quasibound states for that system for total angular momentum $J = 0$. With an increase in the value of J, the depth of the effective potential well and the number of bound states would decrease. The presence of the deep potential well is expected to influence the inelastic and proton-exchange reaction cross sections, especially at low energies, as we shall further discuss later. Plots of inelastic and exchange reaction probability values as a function of collision energy (given in the supplementary material) reveal a large number of resonances, particularly for low J values. However, the weighted sum over J values while computing the cross sections smears out most of the oscillations. Some oscillations do survive J-averaging as it also becomes evident in the plots shown in the present discussion of our results reported below. Rate coefficients obtained by averaging over energies exhibit no oscillations when plotted as a function of the temperature (T). They initially rise rapidly with an increase in T and level off at higher T values, as will be clearly shown in the figures below (e.g., see Fig. 8).

The use of 3D potential energy surfaces allows for the study of vibrational and rotational energy transfer through inelastic collisions and for the occurrence of the (non-observable) exchange process described as follows:

$$HeH^+ + He' \longrightarrow He + He'H^+, \tag{3}$$

where the prime superscript on one of the helium atoms distinguishes it from the other (physically indistinguishable) He atom. The cross section for rotational excitation through the exchange pathway was found to be considerably less than that for the purely inelastic pathway in our earlier work of Gianturco *et al.*[12] Hence, the sum of the cross section values for the inelastic and exchange processes on the PS-PES, which resulted in rotational excitation of HeH^+, turned out to be comparable to the cross sections for the purely inelastic process obtained using the RR-PES, as discussed by Gianturco *et al.*[12] This type of behavior of the flux redistribution among different channels is also observed in the present calculations reported below.

In the present paper, we, therefore, investigate the efficiency of the state-changing rate coefficients pertaining to rovibrationally inelastic collisions between HeH^+ and He under ISM conditions. We shall be using a new 3D *ab initio* surface that explicitly includes the dependence of the potential on the vibrational coordinate (r) of HeH^+, hereinafter referred to as the VR-PES, and we shall also employ the reactive PS-PES presented in the earlier studies by Panda and Sathyamurthy[13] to further investigate the role of the proton-exchange channels in the presence of rovibrational state-changing processes.

II. THE NEW 3D POTENTIAL ENERGY SURFACE

Calculations were carried out using the MOLPRO suite of quantum chemistry codes[18,19] at the coupled-cluster single-double triple and (perturbative) triple excitations [CCSD(T)] level of theory[20,21] employing an aug-cc-pV5Z basis set.[22,23] The expectation value of the non-relaxed CCSD(T) dipole moment at each r distance was also obtained, as further discussed below. More specifically, the *ab initio* approach with the CCSD(T) method extended the aug-cc-pV5Z basis set to the complete basis set (CBS) limit. The calculations included the necessary three coordinates, i.e., the vibrational coordinate (r) of HeH^+, the distance R from the center-of-mass (c.o.m.) of HeH^+ to the He atomic partner, and the angle θ formed between the R and r vectors. The vibrational coordinate was varied between $r = 0.55$ and 1.30 Å covering a range of 14 values, which allowed us to span the vibrational levels of the isolated cation up to the v = 4 excited state. The values of θ went from 0° to 180° over an evenly spaced set of 19 values. For each angular cut, the range of the radial coordinate R went from 1.00 to 10.00 Å covering a total set of 15 050 computed points describing the new VR-PES of the present study.

The LEVEL program[24] was used to obtain the vibrational energies and wavefunctions for the HeH^+ partner molecule. The *ab initio* energies were used as input, interpolated using a cubic spline and extrapolated to r values below and above the range of calculated energies using functions implemented in LEVEL. In the vibrational coupled-channel (VCC) dynamics implemented here and discussed below in more details, we have included relative energies of the first four vibrational levels along with the rotational constants for each

Published under an exclusive license by AIP Publishing

state as shown in the discussion below and compared with previously published and calculated theoretical and experiment values. The agreement with previous calculations and experimental values is quite good and certainly sufficient to evaluate the cross sections and rates constants of the inelastic collisions considered in the present study.

The three-dimensional PESs were fit to an analytical form using the method of Werner, Follmeg, and Alexander[25] and Balança and Dayou[26] where the interaction energy is given as

$$V_{\rm int}(R,r,\theta) = \sum_{n=0}^{N_r-1}\sum_{l=0}^{N_\theta-1} P_l(\cos\,\theta)A_{\rm ln}(R)(r-r_{eq})^n, \qquad (4)$$

where $N_r = 7$ and $N_\theta = 13$, respectively, are the number of bond lengths r and angles θ in the *ab initio* grid, $P_l(\cos\theta)$ are the Legendre polynomials, and $r_{eq} = 0.744\,15$ Å is the equilibrium bond length of HeH^+. For each bond length r_m and angle θ_k, one-dimensional cuts of the PESs $V_{\rm int}(R,r_m,\theta_k)$ were fit to

$$B_{km}(R) = \exp(-a_{km}R)\left[\sum_{i=0}^{i_{\rm max}} b_{km}^{(i)}R^i\right] - \frac{1}{2}[1+\tanh(R)]\left[\sum_{j=j_{\rm min}}^{j=j_{\rm max}} c_{km}^{j}R^{-j}\right], \qquad (5)$$

where the first set of terms accounts for the short range part of the potential and the second part for the long-range terms combined using the $\frac{1}{2}[1+\tanh(R)]$ switching function. For each r_m and θ_k, Eq. (5) was least-squares fit to the *ab initio* data (around 40 R points) using $i_{\rm max} = 2$, $j_{\rm min} = 4$, and $j_{\rm max} = 10$ for eight variable parameters. The average root-mean-square error (RMSE) for each fit was 1.8 cm^{-1} for the present system. From the 1D potential fits $B_{km}(R)$, the radial coefficients $A_{\rm ln}(R)$ can be determined from the matrix product $\mathbf{A}(R) = \mathbf{P}^{-1}\mathbf{B}(R)\mathbf{S}^{-1}$, where the matrix elements of $\mathbf{P}$ and $\mathbf{S}$ are given as $P_{kl} = P_l(\cos\theta_k)$ and $S_{nm} = (r_m - r_{eq})^n$, respectively.

The analytical fitting of the PES, Eq. (4), gives a reasonable representation of the *ab initio* interaction energies. An overall RMSE of 0.57 cm^{-1} for all points used in the fit was obtained for HeH^+/He for all points with $V < 500$ cm^{-1}.

The scattering calculations described in Sec. III require the interaction potential to be averaged over the vibrational states of $HeH^+\chi_v(r)$, which were obtained from LEVEL as described earlier in this section, as described in the following equation:

$$V_{v,v'}(R,\theta) = \langle\chi_v(r)|V_{\rm int}(R,r,\theta)|\chi_{v'}(r)\rangle. \qquad (6)$$

An interesting visual presentation of the coupling potential in terms of energy maps is given in the four panels reported in Fig. 1. It is clear, for instance, that the map reported by the upper-left panel is very similar to the same map obtained from the RR-PES discussed earlier in our work.[12] It, therefore, indicates that the expected coupling without vibrational excitation channels would produce similar quantum dynamics observables as the PES using the rigid-rotor (RR) approximation. The direct off-diagonal coupling energy map is given in the upper-right panel for the $v = 0$ and = 1 vibrational states and in the lower-right panel for the coupling between the $v = 1$ and $v = 2$ states. One clearly sees there that the coupling

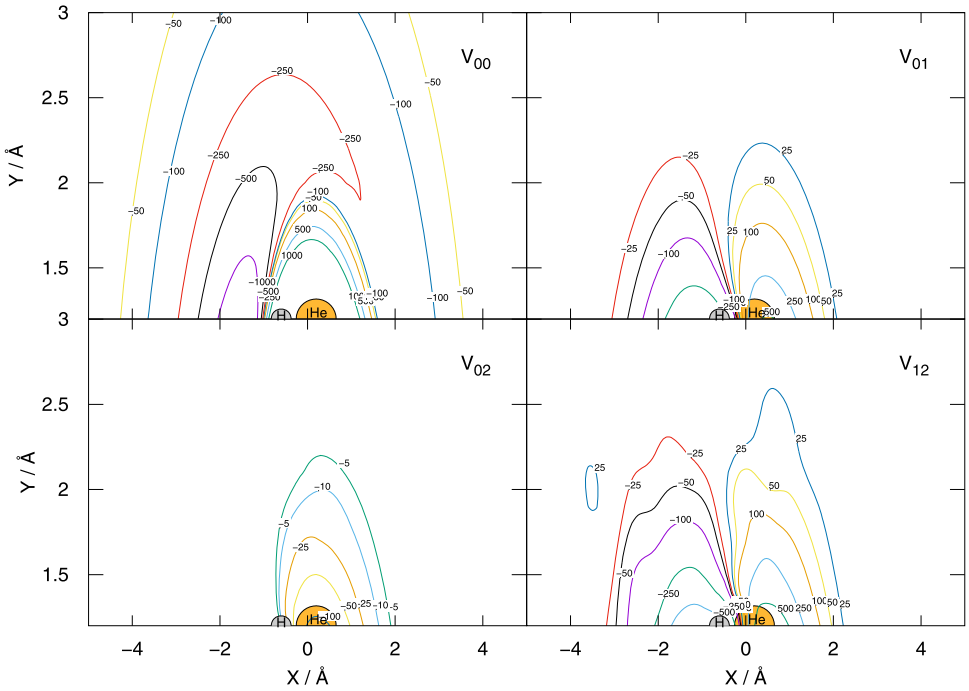


FIG. 1. Computed vibrational coupling PESs associated with the different vibrational states discussed in this work. Each panel presents a 2D energy map of the coupling. Upper-left: the V_{00} diagonal term. Upper-right: the V_{01} direct coupling surface. Lower-left: V_{02} coupling. Lower-right: V_{12} coupling surface. See the main text for further comments.

Published under an exclusive license by AIP Publishing

strength is consistently smaller in the case where the $\Delta v = 2$ transitions are involved, a feature also evident from the map shown in the lower-left panel and involving dynamical coupling between the $v = 0$ and $v = 2$ levels.

The vibrational coupled-channel (VCC) scattering calculations to be discussed in Sec. III require to have the vibrationally averaged (VA) matrix elements in the form of the familiar multipole expansion given as

$$V_{v,v'}(R,\theta) = \sum_{\lambda}^{\lambda_{max}} V^{\lambda}_{v,v'}(R) P_{\lambda}(\cos\,\theta). \tag{7}$$

Figure 2 shows the multipole expansion coefficients for the first three $V^{\lambda}_{v,v'}(R)$ terms and for values of λ associated with the first three

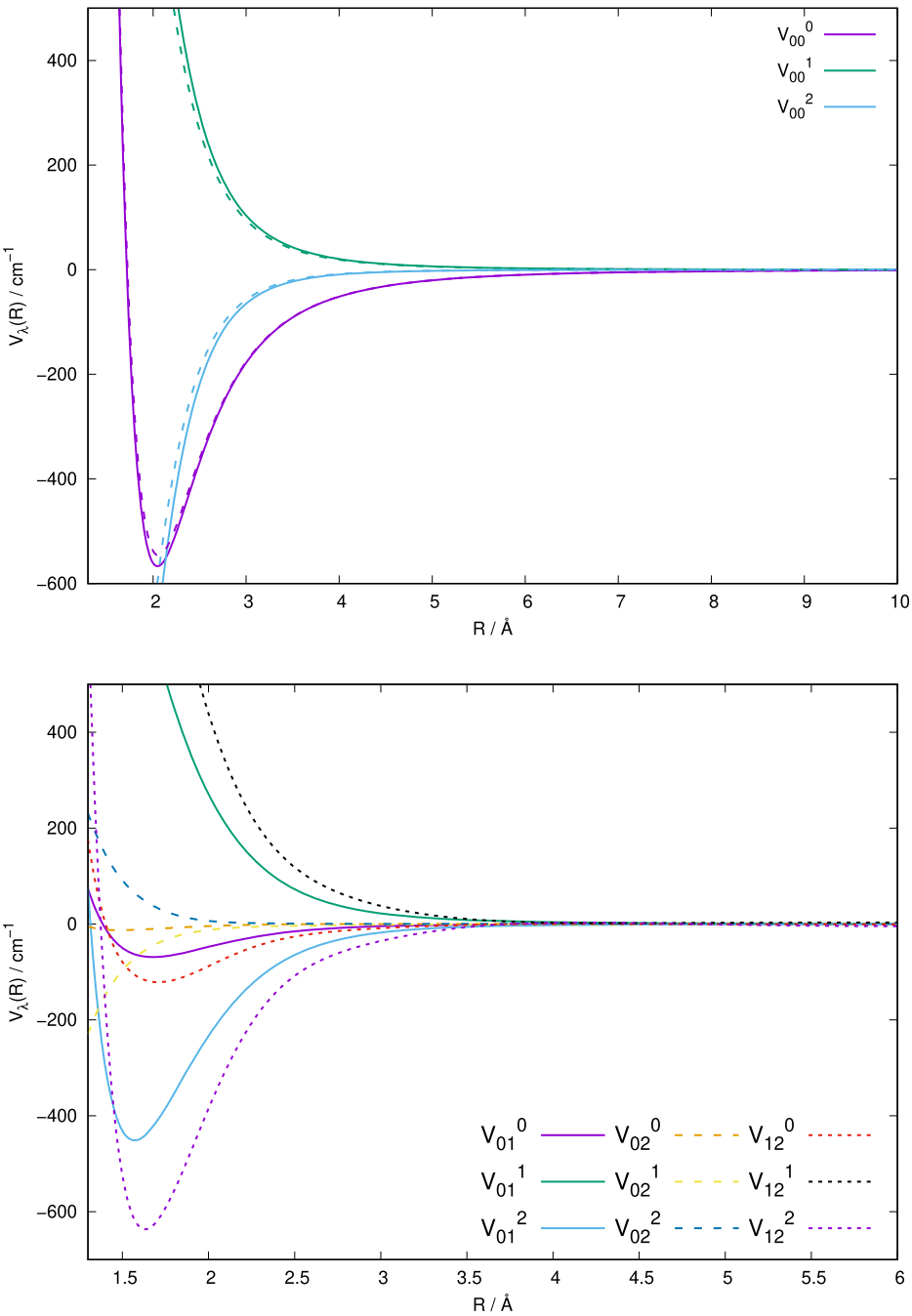


FIG. 2. Vibrationally inelastic Legendre expansion coupling radial coefficients obtained from the *ab initio* calculations of the VR-PES. The dashed lines in the upper panel report the RR-PES curves taken from the work of Gianturco *et al.*[12] See the main text for further details.

Published under an exclusive license by AIP Publishing

expansion terms in Eq. (8). The upper panel also reports the RR-PES for the cation as a rigid rotor (dashed lines).

It is interesting to note from the curves reported in the upper panel of Fig. 2 that the three multipolar coefficients shown there describe the diagonal coupling term for the cation in its ground vibrational level. They represent the vibrationally averaged (VA) version of the 3D potential energy surface where the vibrating cation is in its ground vibrational state. The simpler 2D version of this PES (which was used for the earlier calculations reported in our own work by Gianturco *et al.*[12]) produced the same multipolar coefficients shown in that panel by the dashed lines: we easily see there that the two versions of the interaction are nearly coincident. This indicates that the Rigid-Rotor (RR) version of the PES is essentially unchanged when its VA version is employed, thereby indicating that the RR-type of calculations would realistically describe the rotationally inelastic dynamics when the vibrating cation remains in its ground vibrational state.

The off-diagonal coupling terms from the multipole expansion of Eq. (8) are given by the curves in the lower panel of Fig. 2. We also see there that the coupling potential terms between levels connected by a $\Delta v = 1$ transition are the strongest terms and their spherical contributions are also the strongest. Such behavior would suggest that vibrational excitation processes between neighboring levels would be the stronger processes, as we shall, in fact, show below.

III. THE QUANTUM VIBRATIONAL DYNAMICS

Quantum scattering calculations were carried out using the VCC method to solve the Schrödinger equation for scattering of an atom with a diatomic molecule as implemented in our in-house code, ASPIN.[27] The method has been described in detail many times before, from one of its earliest, now classic formulations,[28] to one of its more recent, the computation-oriented form of our own version.[27] Therefore, only a brief summary will be given below, with all equations given in atomic units.

By starting with the form of any given total angular momentum $\mathbf{J} = \mathbf{l} + \mathbf{j}$, the scattering wavefunction is expanded as

$$\Psi^{JM}(R, r, \theta) = \frac{1}{R}\sum_{v,j,l} f^{J}_{vlj}(R)\chi_{v,j}(r)\mathcal{Y}^{JM}_{jl}(\hat{\mathbf{R}}, \hat{\mathbf{r}}), \tag{8}$$

where l and j are the orbital and rotational angular momentum, respectively, and $\mathcal{Y}^{JM}_{jl}(\hat{\mathbf{R}}, \hat{\mathbf{r}})$ are coupled-spherical harmonics for l and j, which are eigenfunctions of J. $\chi_{v,j}(r)$ are the radial part of the rovibrational eigenfunctions of the cation. The values of l and j are constrained, via Clebsch–Gordan coefficients, such that their final summation is compatible with the specific total angular momentum J under consideration.[27,28] $f^{J}_{vlj}(R)$ are the radial expansion functions, which need to be determined from the propagation of the radial coupled equations.

Substituting the expansion into the Schrödinger equation with the Hamiltonian for atom–diatom scattering, as detailed in Refs. 27 and 28, leads to the CC equations for each contributing total angular momentum J,

$$\left(\frac{d^2}{dR^2} + \mathbf{K}^2 - \mathbf{V} - \frac{\mathbf{l}^2}{R^2}\right)\mathbf{f}^{J} = 0. \tag{9}$$

Here, each element of $\mathbf{K} = \delta_{i,j} 2\mu(E - \epsilon_i)$ (where ϵ_i is the channel asymptotic energy), μ is the reduced mass of the system, $\mathbf{V} = 2\mu\mathbf{U}$ is the interaction potential matrix between channels, with the matrix $\mathbf{U}$ containing the actual potential terms, and $\mathbf{l}^2$ is the matrix of orbital angular momentum. For the rovibrational scattering calculations of interest in the present study, the matrix elements $\mathbf{V}$ are given explicitly as

$$\langle vjlJ|V|v'j'l'J\rangle = \int_0^\infty dr \int d\hat{\mathbf{r}} \int d\hat{\mathbf{R}} \chi_{v,j}(r)\mathcal{Y}^{JM}_{jl}(\hat{\mathbf{R}}, \hat{\mathbf{r}})^* \times V(R, r, \theta)\chi_{v',j'}(r)\mathcal{Y}^{JM}_{j'l'}(\hat{\mathbf{R}}, \hat{\mathbf{r}}). \tag{10}$$

Since the intermolecular potential $V(R, r, \theta)$ is expressed as in Eq. (7), then Eq. (10) can be written as

$$\langle vjlJ|V|v'j'l'J\rangle = \sum_{\lambda=0}^{\infty} V^{\lambda}_{v,v'}(R) f^{J}_{\lambda jlj'l'}, \tag{11}$$

where the $f^{J}_{\lambda jlj'l'}$ terms are the Percival–Seaton coefficients,

$$f^{J}_{\lambda jlj'l'} = \int d\hat{\mathbf{r}} \int d\hat{\mathbf{R}} \quad \mathcal{Y}^{JM}_{jl}(\hat{\mathbf{R}}, \hat{\mathbf{r}})^* P_\lambda(\cos\theta)\mathcal{Y}^{JM}_{j'l'}(\hat{\mathbf{R}}, \hat{\mathbf{r}}), \tag{12}$$

for which analytical forms are known.[27] Equation (11) also makes use of the widely known approximation

$$V^{\lambda}_{v,v'}(R) \approx V^{\lambda}_{vjv'j'}(R) \tag{13}$$

for all j so that the effect of rotations on the vibrational matrix elements is largely ignored for reasons that shall be further discussed below.

The VCC equations are propagated outward from the classically forbidden region to a sufficiently large relative distance where the scattering matrix $\mathbf{S}$ can be obtained. The inelastic rovibrational state-changing cross sections are obtained as

$$\sigma_{vj\to v'j'} = \frac{\pi}{(2j+1)k^2_{vj}}\sum_J (2J+1)\sum_{l,l'}|\delta_{vlj,v'l'j'} - S^{J}_{vlj,v'l'j'}|^2. \tag{14}$$

To converge the VCC equations, a rotational basis set was also used: it included up to j = 18, 17, and 15 rotational functions for the v = 0, 1, and 2 coupled vibrational states. The VCC equations were propagated between 1.0 and 80.0 Å using the log-derivative propagator[29] up to 50 Å and the variable-phase (VP) method at larger distances.[30] The potential energy was interpolated between the calculated $V^{\lambda}_{v,v'}(R)$ values using a cubic spline. For $R > 10$ Å, $V^{\lambda}_{v,v'}(R)$ for the $\lambda = 0$ term was extrapolated as $\frac{c}{R^4} + \frac{d}{R^6}$. As our *ab initio* calculated raw-point energies were obtained up to $R = 10$ Å and extrapolated with the above long-range form of the ion-neutral interaction coefficients for $R > 10$ Å (see the work of López-Durán, Bodo, and Gianturco[27]) where the interaction energy is negligible for the temperatures of interest here, the extrapolated form was also found to have a negligible effect on the converged cross sections.[31]

A number of parameters of the calculation were checked for convergence. For production calculations, 13 λ terms were included for each $V_{v,v'}(R)$ as a compromise between accuracy and computational time.

Scattering calculations were carried out for total energies between 1 and 8000 cm^{-1}. Different steps were considered depending on the energy range (from 1.0 cm^{-1} for lowest energies up to 100 cm^{-1} for the largest ones) for ensuring that important features

Published under an exclusive license by AIP Publishing

as resonances appearing in the cross sections were accounted for and their contributions included when the corresponding rates were calculated. At low collision energies, the positions and widths of such resonances will be very sensitive to the details of the PES. The number of partial waves was increased with increasing energy as usual, requiring $J = 150$ for the highest energies considered.

Rovibrational inelastic cross sections for HeH^+ ($v = 1, 2$ and $j = 0$) going to HeH^+ ($v = 0, 1, 2$ and j' = all open rotational states for each total energy) were computed using the quantum method outlined above and employing the new VR-PES also discussed in Sec. II.

The (HeH^+/He) rovibrational dynamics was also carried out using the PS-PES that we have described in detail in our earlier work.[12] The calculations were done using the ABC code as detailed by Skouteris, Castillo, and Manolopoulos[32] for $v = 0$, 1, and 2 and $j = 0$ in the ionic partner HeH^+ over a broad range of E_{trans} that will be detailed in Sec. IV. The relevant code parameters used in our present calculations are specified as follows: the maximum energy (Emax) = 2.50 eV in any channel and a maximum (jmax) of 17 rotational states. We have considered the maximum of hyperradius (Rmax) to be 24 a_0, with the number of log-derivative propagation sectors (MTR) = 250, the total angular momentum (Jtotmax) going up to 90, and the helicity truncation parameter (Kmax) = 1. It should be noted that the present results are essentially the same as those obtained earlier in reactive scattering studies that were also discussing the title system; see the work of Liang *et al.*[14]

The necessary state-to-state cross sections ($\sigma_{v,j}^{v',j'}$) for vibrationally inelastic processes, with the HeH^+ internal states going from the $v = 1, j = 0$ state to the $v' = 0, j' = 0$–17 states, were computed over the E_{trans} range between 42 and 6000 cm^{-1}. For the $v = 2$, $j = 0$ state going to $v' = 1$, $j' = 0$–16 and $v' = 0$, $j' = 0$–17 states, the calculations were carried out over the E_{trans} range between 21 and 3400 cm^{-1}.

The computed results for cross sections and inelastic rate coefficients were obtained using both the 3D potential energy surfaces discussed in this work, and the details of the present findings will be given and discussed in Sec. IV.

IV. RESULTS AND DISCUSSION

A. Comparing cross section calculations on the VR-PES and the PS-PES

Inelastic transition probability (P_{in}) values obtained via the PS-PES discussed earlier and from the reactive/inelastic calculations that employed the ABC code of Skouteris, Castillo, and Manolopoulos[32] have been produced for initial ($v = 0, 1, 2, j = 0$) and final ($v' = 0, 1, 2, j' = 0, \ldots, 17$) states of the HeH^+ cation, given as a function of E_{trans} for different total angular momentum (J) values: their specific values are provided in the supplementary material. The presence of numerous oscillations in the P_{in} vs E_{trans} plots is found, as generally expected, to get largely quenched when the state-to-state cross sections ($\sigma_{v,j}^{v',j'}$) are calculated by summing P_{in} over the J values,

$$\sigma_{v,j}^{v',j'} = \sum_J (2J+1) P_{in}\left(v, j \to v', j'; E_{trans}, J\right). \tag{15}$$

The specific values we have obtained for $\sigma_{v,j}^{v',j'}$ in the initial $v = 1$, $j = 0$ state and going to $v' = 0$, with j' varying from 0 to 11, are plotted as an example of the present results. They are given as a function of E_{trans} in Fig. 3, where the computations used the PS-PES interaction via the ABC code, as mentioned earlier.

One can easily note that for all the $j' = 0$–9 states in Fig. 3, the $\sigma_{v,j}^{v',j'}$ values are the largest at the lowest E_{trans}, decreasing by more than one order of magnitude as E_{trans} is increased to 6000 cm^{-1}. Furthermore, since the energy gap between transitions from the initial to the final states considered becomes the largest for $j' = 0$, the ensuing computed cross sections turn out to be the smallest for $j' = 0$.

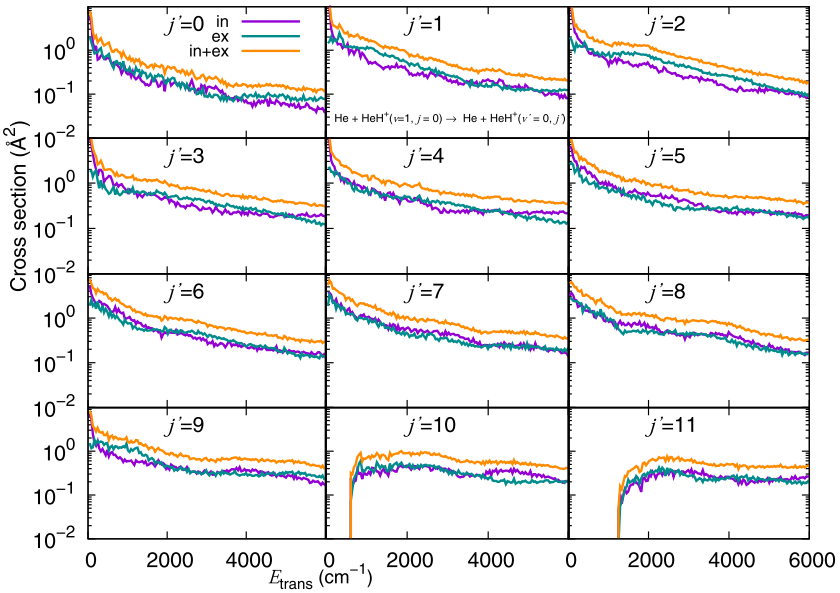


FIG. 3. Integral inelastic cross sections obtained by including either the purely inelastic (labeled in) channel or the proton-exchange (labeled ex) reactive channel. The results with the sum of the two separate channels are labeled in + ex. All the present calculations for HeH^+ ($v = 1$, $j = 0$) + He → HeH^+ ($v' = 0, j'$) + He were obtained from the PS-PES using the ABC code.

Published under an exclusive license by AIP Publishing

On the other hand, as the final j' is increased, there is also a noticeable increase in the $\sigma_{v,j}^{v'j'}$ values, a feature which does not change much when going to the higher j' final states. This has to do with at least two factors in the inelastic dynamics: (i) as the final j' increases, the energy gap between the initial and final states decreases, thereby making the energy-transfer dynamics more favorable. Additionally, the degeneracy of the final j' state increases, thereby adding more flux contributions to the final inelastic probabilities.

It is also important to point out at this stage that for transitions to states with $j' = 10$ and above, there is an energetic threshold that increases with increasing j'. This is understandable as the energy of the j' state ≥10 is higher than the initial state $v = 1, j = 0$. A pictorial view of these differences is presented by the plots in Fig. 4. The actual values shown there come from using the PS-PES. However, as discussed in detail in Sec. II, the sequence of rovibrational states of the same cation given via the new VR-PES presented here are essentially the same.

The state-to-state inelastic cross sections can also be computed for the exchange pathway described by Eq. (4), which is also leading to any of the $(v' = 0, j')$ states discussed earlier. The present calculations show that the size of the related cross sections is, indeed, comparable in magnitude to that we have found for the purely inelastic cross sections for the same $(v' = 0, j')$ state: this is illustrated by the data also reported in the panels of Fig. 3.

Since the two pathways of the proton-exchange reaction are physically not distinguishable, we present in Fig. 3 the sum of the two separately computed channels as the true observable inelastic cross sections for each of the (v', j') final states.

The fact that the exchange reaction contributes significantly when compared to the purely inelastic collision pathway in vibrationally inelastic processes has been discussed for a long time in a variety of "potentially reactive" atom–diatom systems.[33] In the case of the purely rotationally inelastic cross sections for (HeH^+, He) collisions, which we had reported in our earlier paper by Gianturco *et al.*,[12] there was also a sizable contribution to the energy-transfer processes coming from the exchange reaction route, but that amount was considerably less in magnitude when compared to the purely inelastic pathway. We thus found in that study that the sum of the cross sections for the two pathways yielded values comparable to the purely inelastic cross sections computed using the RR model, thus justifying the use of only the nonreactive channels for computing rotationally inelastic cross sections, as we shall further discuss below in the case of vib-rotational inelastic processes.

Inelastic cross section values for both pathways and for the sum of the two, this time involving HeH^+ ($v = 2, j = 0$) going to $v' = 1$ and $j' = 0$–11, are plotted as a function of E_{trans} in Fig. 5. It is clear that the results in Fig. 5 exhibit similar trends as noted for the $v = 1$, $j = 0$ state of HeH^+ (see Fig. 3). Hence, it means that the exchange pathway contributes as much as the purely inelastic pathway to the data reported now in Fig. 5 and that the $\Delta v = -1$ cross section values starting at $v = 2, j = 0$ are comparable in magnitude to the processes initiated at $v = 1, j = 0$. We also note here that for the $v = 2, j = 0$ initial state, there is again a translational threshold when going to $j' = 10$, as observed before in Fig. 3.

A similar type and range of cross section results as those analyzed in Figs. 3 and 5 are now presented in Fig. 6, but this time looking at vibrational cooling processes associated with the $\Delta v = -2$ transitions. There is a noticeable drop in the size values of these cross sections, as should be expected when the energy gaps increase for the transitions, thereby making the energy-transfer dynamics less efficient. Apart from their smaller size, however, the results plotted in Fig. 6 behave largely as those plotted in Figs. 3 and 5 in all aspects, except for the translational threshold now moving to $j' \geq 13$ (not shown, however, in Fig. 6).

The integral inelastic cross sections computed using the new VR-PES, described in Sec. II, are now presented and compared with the corresponding results obtained on the PS-PES in Figs. 3, 5, and 6. We see in Fig. 7 that there are some differences in the energy dependence for the transitions from the $v = 1, j = 0$ state down to $v' = 0$ and different final rotational states (some of which are shown

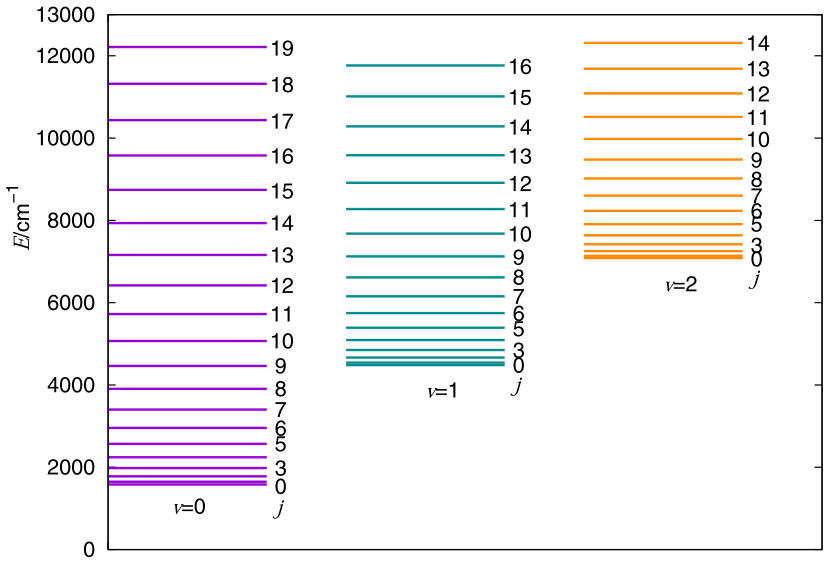


FIG. 4. Vib-rotational energy level diagram for HeH^+ obtained using the diatomic potential from the PS-PES. The values are essentially the same as those from the VR-PES calculations discussed in the main text.

Published under an exclusive license by AIP Publishing

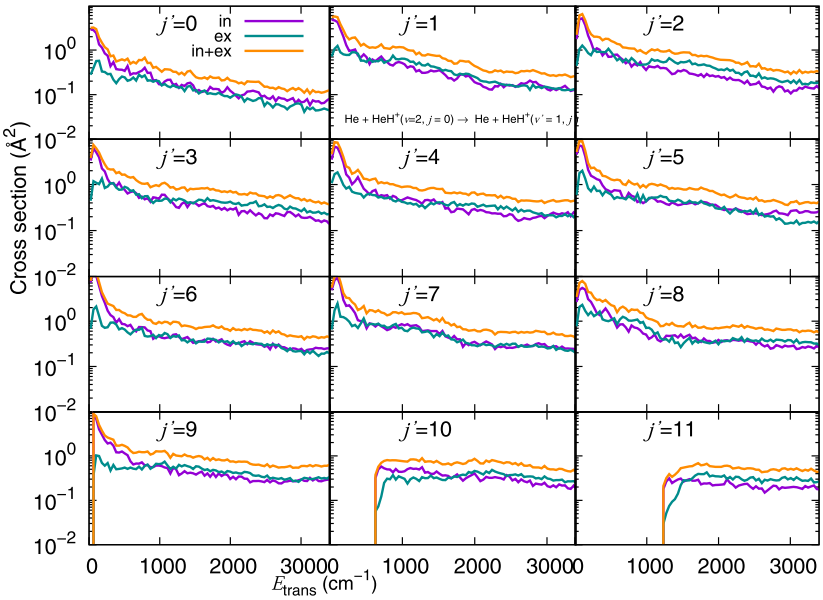


FIG. 5. Same as in Fig. 3 but here for the HeH^+ ($v = 2, j = 0$) + He → HeH^+ ($v' = 1, j'$) + He processes, again obtained from the quantum dynamics calculations on the PS-PES interaction using the ABC code.

in Fig. 7), although the results obtained using the VR-PES are largely comparable to those obtained using the PS-PES and including both channels. One of the important findings from this comparison is that the purely inelastic process on the new 3D VR-PES is very close in size to what was found earlier from including both the inelastic and the proton-transfer channels, indicating that in the end, the inclusion of the reactive channels is not altering the general size of the rovibrational cooling processes for the present cation.

If we now move to the data reported in Fig. 8, we can clearly see that the results obtained using both the PESs of the present work are very much comparable for the $v = 2, j = 0 \rightarrow v' = 1, j' = 0$–5 transitions.

However, there are noticeable differences between the two sets of results for $v = 2, j = 0 \rightarrow v' = 0, j' = 0$–5 transitions, as can be seen in Fig. 9.

In order to summarize the general trend of the rovibrational de-excitation (cooling) transitions, the data presented in Fig. 10 now compare the relative sizes and energy behavior of the rovibrational cooling processes, indicating the $\Delta v = -1$ transitions summed over all the final rotational states opened at each collision energy considered. As expected from the energy-gap simple rule, we clearly see that the larger the gap, the less efficient the cooling process of the cation by collisions with He atoms. This also means that de-excitation paths by collision involving contiguous vibrational levels

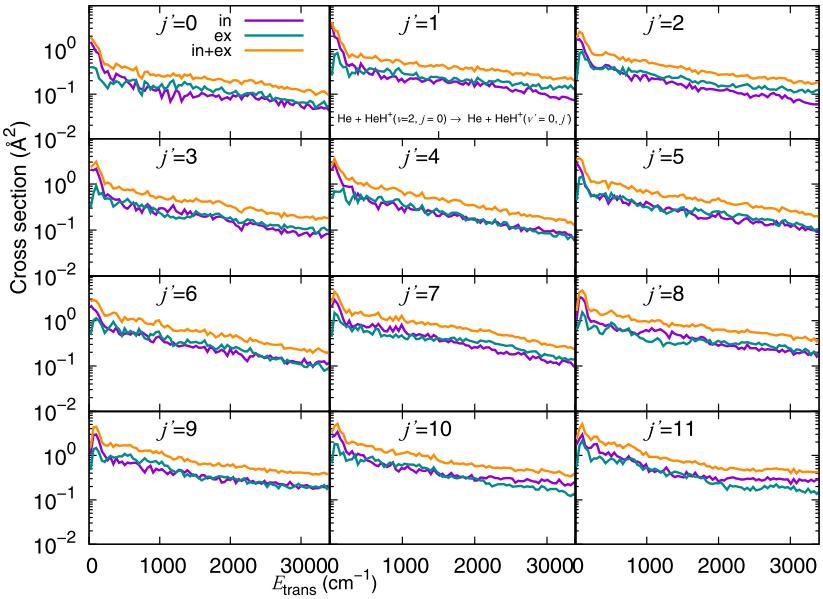


FIG. 6. Integral inelastic cross sections through the purely inelastic channel and the exchange channel and the sum of the two for HeH^+ ($v = 2, j = 0$) + He → HeH^+ ($v' = 0, j'$) + He as a function of E_{trans}, as obtained from close-coupling calculations on the PS-PES.

Published under an exclusive license by AIP Publishing

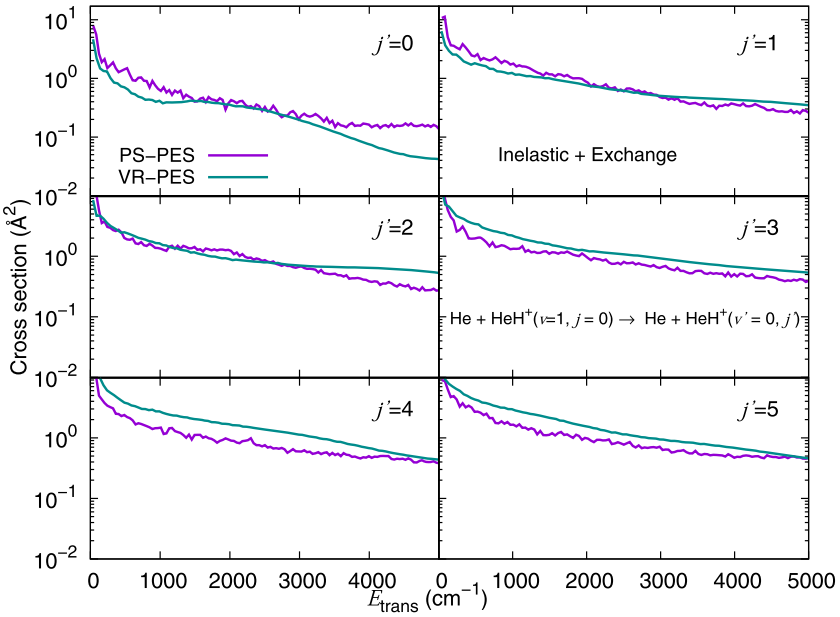


FIG. 7. Comparison of the inelastic cross sections computed on the VR-PES and PS-PES for HeH^+ ($v = 1$, $j = 0$) → HeH^+ ($v' = 0$, $j' = 0$–5) transitions due to collisions with He. The results on the PS-PES include the purely inelastic channel and the exchange channel.

are more efficient than those where further apart vibrational states are involved, as seen in the data from Fig. 9. We further see in the two panels of Fig. 10 that the two PESs considered in this study yield overall energy-transfer flux, which is remarkably similar at all the considered energies for the two interactions. Additionally, our calculations numerically verify that in the case where the proton-exchange channels are included via the ABC code with the PS-PES interaction, the purely inelastic component is accordingly reduced in size to produce the (in + ex) sum, which is essentially the same as that obtained when the purely inelastic scattering code is employed via the VR-PES interaction. These findings indicate that the important de-excitation processes for the present cation yield in both cases large TOTAL energy-exchange flux distributions into the environmental baryons exemplified in this study by the abundant He atoms.

B. Vibrational de-excitation rate coefficients on the VR-PES and the PS-PES

The rate coefficients involving the different de-excitation processes were computed using the standard definition

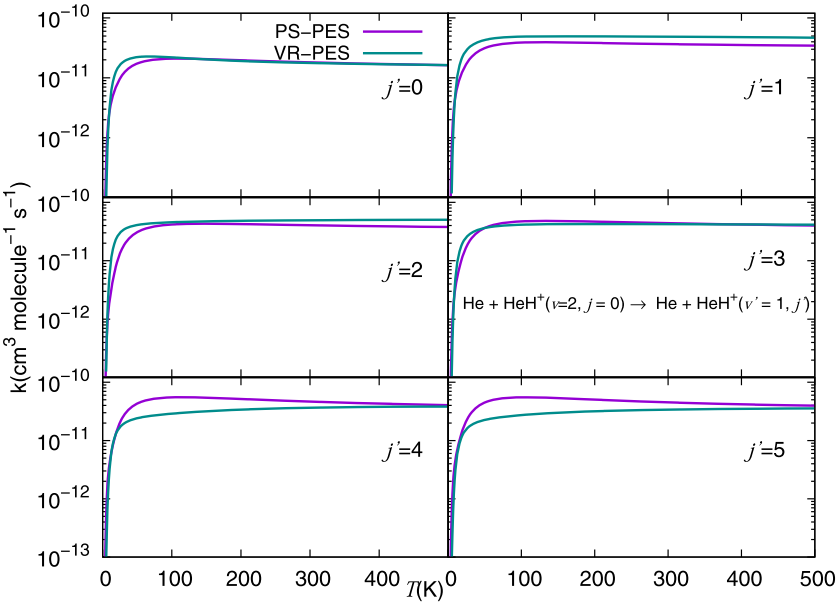


FIG. 8. Comparison of the inelastic cross sections computed on the VR-PES and PS-PES for HeH^+ ($v = 2$, $j = 0$) → HeH^+ ($v' = 1$, $j' = 0$–5) transitions due to collisions with He. The results on the PS-PES include the purely inelastic channel and the exchange channel.

Published under an exclusive license by AIP Publishing

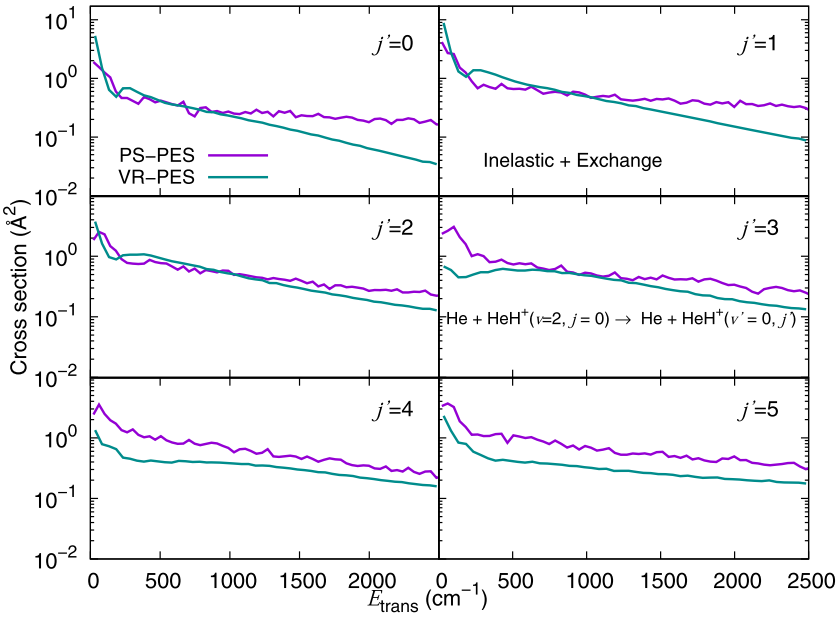


FIG. 9. Comparison of the inelastic cross sections computed on the VR-PES and PS-PES for HeH^+ ($v = 2$, $j = 0$) → HeH^+ ($v' = 0$, $j' = 0$–5) transitions due to collisions with He. The results on the PS-PES include the purely inelastic channel and the exchange channel.

$$k_{v,j\to v',j'}(T) = \left(\frac{8}{\pi\mu k_B^3 T^3}\right)^{1/2} \int_0^\infty E_{\text{trans}} \sigma_{v,j}^{v',j'}(E_{\text{trans}}) e^{-E_{\text{trans}}/k_B T} dE_{\text{trans}} \tag{16}$$

over the temperature range from 1 to 500 K.

We present below the computed rate coefficients (k) for different vibrationally inelastic (de-excitation or cooling) processes for

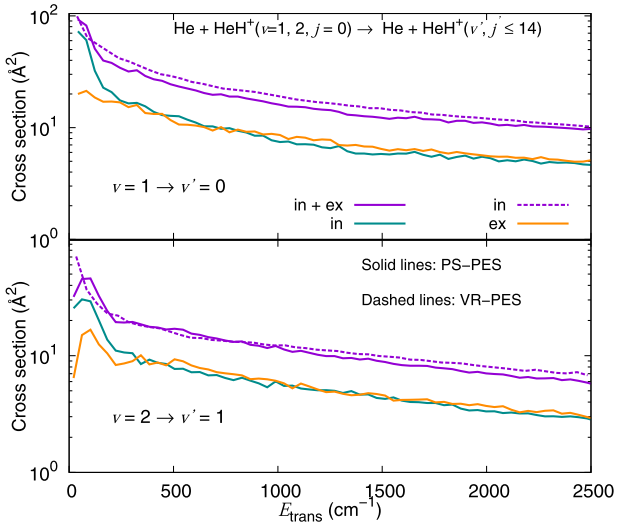


FIG. 10. Integral inelastic cross sections involving rovibrational de-excitation paths of HeH^+, from $v = 1$, $j = 0$ to $v' = 0$ and from $v = 2$, $j = 0$ to $v' = 1$. The final channels are summed over all the final j' channels open at each considered energy up to $j' = 14$. The different processes are color-coded in the panels. The quantum calculations are on the PS-PES and the VR-PES using the ABC and the ASPIN codes, respectively. See the main text for further details.

[HeH^+ ($v = 1, 2$, $j = 0$), He] collisions within the temperature range between 1 and 500 K. The data are shown in Figs. 11–13.

It is clear from Fig. 11 that the k value for $v = 1$, $j = 0$ → $v' = 0$, $j' = 0$–8 transitions for HeH^+ increases from ~ 10^{-12} to 6×10^{-11} cm^3 $molecule^{-1}$ s^{-1} as T increases from 10 to 500 K and j' increases from 0 to 8. The cooling rate coefficients are the smallest for $j' = 0$ and the highest for $j' = 8$ at the high end of the temperature scale. As already discussed for the corresponding cross sections earlier, the energy-transfer processes become more efficient as the energy gaps involved in the energy being exchanged become smaller. They further increase in size very rapidly from the threshold up to about 100 K, while for the higher T values, their sizes remain largely the same.

Similar results are obtained for HeH^+ ($v = 2$, $j = 0$) → ($v' = 1$, $j' = 0$–8) transitions, as illustrated in Fig. 12. We see there, in fact, that the rate coefficients are the smallest for $j' = 0$ and increase progressively (not necessarily linearly) with j', reaching their largest values for $j' = 8$. One can also note, however, that the overall sizes of these rates are larger than those reported by Fig. 11, an effect associated with the reduced energy gap between the two main vibrational states of these transitions as opposed to those given in Fig. 11. The difference can be readily checked by the data reported in Fig. 4.

When we next look at the transitions involving the $v = 2$, $j = 0 \to v' = 0, j' = 0$–8 transitions, reported in Fig. 13, we can see that the corresponding computed k values are once more the smallest for $j' = 0$ and the largest for $j' = 8$. In addition, it can be seen that these rate coefficients are noticeably smaller since we are now increasing the main vibrational energy gap when looking at $\Delta v = -2$ transitions in comparison to the quantities, shown in Figs. 11 and 12, where $\Delta v = -1$ transitions were discussed.

To further extend the comparison with the results we have obtained when using the VR-PES discussed in Sec. IV A, we now show state-to-state rate coefficients computed with the two PESs with the data in Fig. 14. In the six panels of Fig. 14, we are

Published under an exclusive license by AIP Publishing

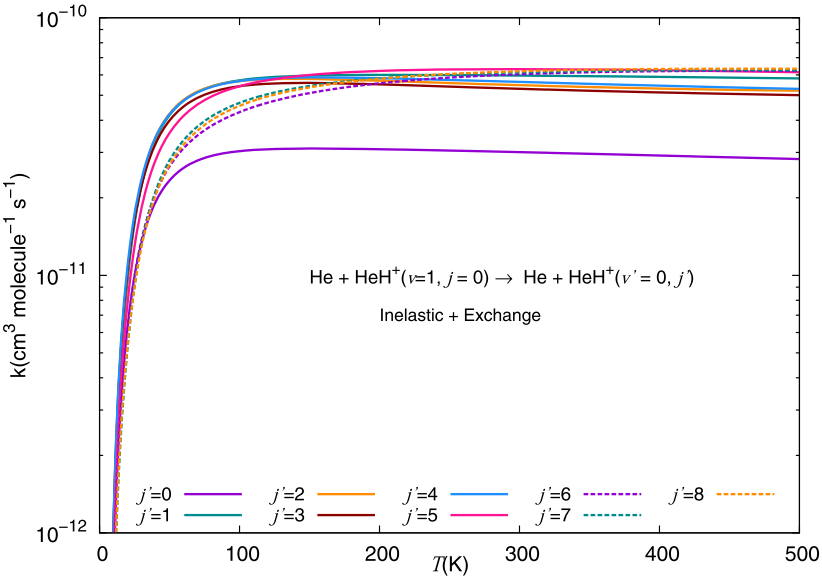


FIG. 11. Rate coefficients for transitions from HeH^+ (v = 1, j = 0) to HeH^+ (v' = 0, j' = 0–8) on collision with He over a range of temperature, computed using the PS-PES.

comparing the relative sizes and temperature dependence for a selection of the final rotational states reached during the de-excitation (cooling) processes from the (v = 1, j = 0) to the (v' = 0, j' = 0–5) final levels. Because the calculations involving the reactive scattering code ABC (and using the PS-PES potential) also include the proton-exchange channels besides the inelastic channels, we see that in the cooling processes with the largest energy gap (e.g., that in the upper-left and upper-right panels of Fig. 14), the presence of the reactive channels increases above about 50 K the overall size of the rate coefficients with respect to the case where the purely inelastic channels are considered through the use of the VR-PES and the scattering code ASPIN discussed earlier. The difference, however, is not very large and becomes increasingly smaller when the involved energy gaps are reduced and both rate coefficients become bigger. This is a significant result that indicates that the efficiency of the collision-exchanged internal energy is large for both the PESs we are using, and despite the differences in the method used for the dynamics, the similarities already indicated between the two PESs cause both the set of calculations to produce remarkably similar final results for the inelastic rates.

For v = 2 → 1 transitions, the energy gap is now reduced with respect to the previous cases illustrated in Fig. 14 so that the k values obtained on the two PESs are now slightly larger and very close to each other, as seen in Fig. 15. Here, again, we verify that the

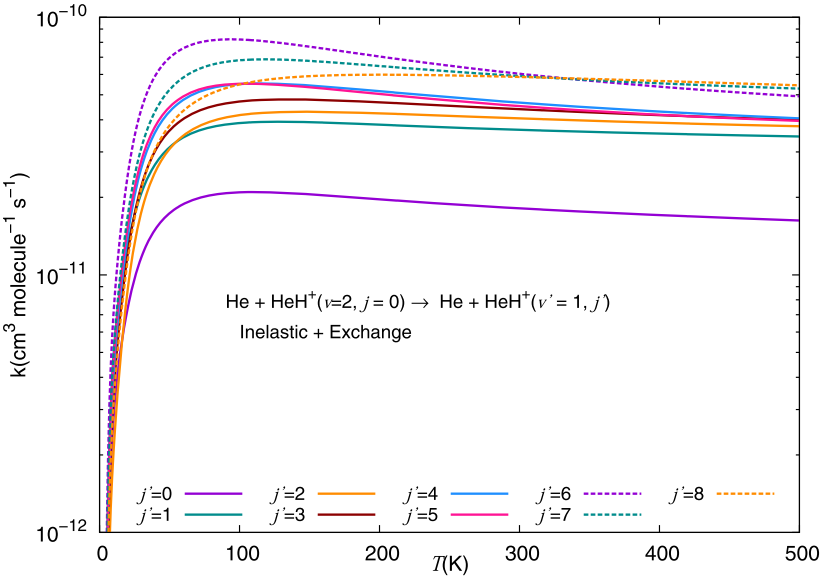


FIG. 12. Rate coefficients for transitions from HeH^+(v = 2, j = 0) to HeH^+(v' = 1, j' = 0–8) on collision with He over a range of temperature, computed using the PS-PES.

Published under an exclusive license by AIP Publishing

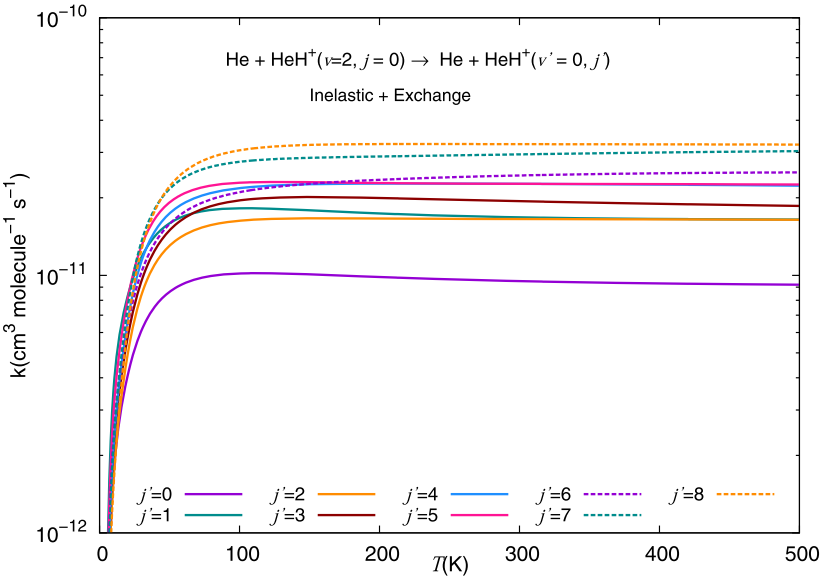


FIG. 13. Rate coefficients for transitions from HeH^+ ($v = 2, j = 0$) to HeH^+ ($v' = 0, j' = 0$–8) on collision with He over a range of temperature, computed using the PS-PES.

inclusion of the reactive channels as done via the PS-PES interaction produces rate coefficients, which are slightly larger than those obtained via the VR-PES interaction without the reactive channels. However, given the differences in both interaction potentials and the employed quantum dynamics, it is very considerable to discover that both the set of processes come out to be rather close in size and T-dependence. We also note here that slightly smaller rate coefficients are obtained for the case of the $\Delta v = 2$ transitions from $v = 2$ to $v = 0$. These coefficients also are shown to present very similar T-dependence from calculations carried out on either of the present PESs and reported in Fig. 16.

In summary, there are fairly minor differences in the k values, which we have obtained from using either of the two PESs, but basically both results indicate strong similarities and very similar general trends of their relative size, temperature dependence, and dependence on the vibrational energy transfer and on the final rotational state of the cooled cation. When the rovibrational energy-transfer processes also include the proton-exchange channel, through the use of the PS-PES and the ABC reactive code, they uniformly generate slightly larger de-excitation rates, which are, indeed, expected from the previous analysis of the corresponding inelastic vs reactive cross sections.

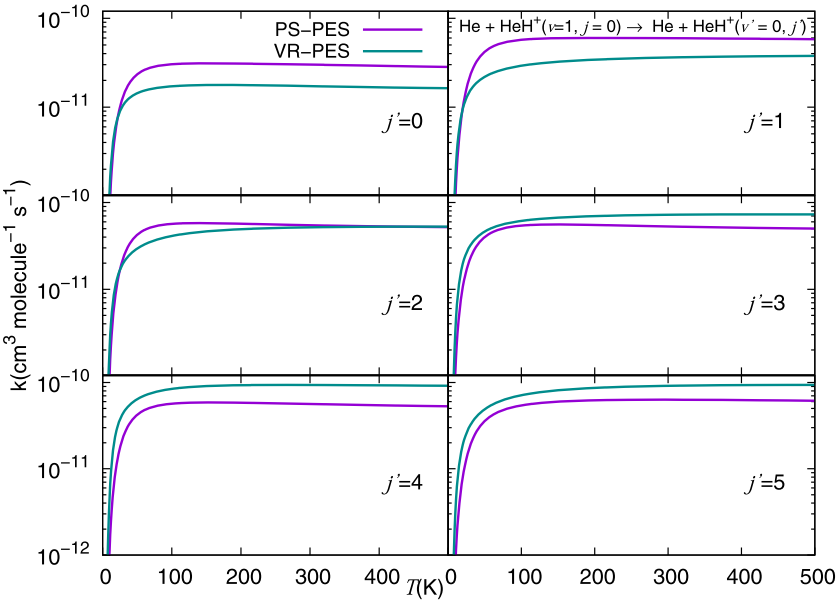


FIG. 14. Comparison of the rate coefficients obtained for transitions from ($v = 1, j = 0$) to ($v' = 0, j' = 0$–5) on collision with He and over the same range of temperatures shown in the previous figures. The data using either the VR-PES or the PS-PES are shown by different colors and labeled in each panel.

Published under an exclusive license by AIP Publishing

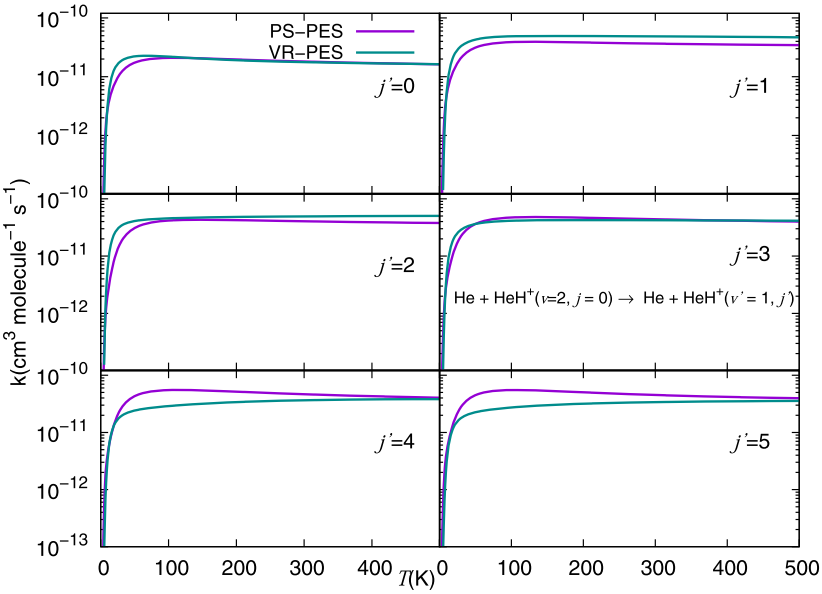


FIG. 15. Same data as in Fig. 14 but for transitions from $HeH^+(v = 2, j = 0)$ to $HeH^+(v' = 1, j' = 0–5)$ on collision with He over the same range of temperature. The labeling in each panel refers to using either the VR-PES or the PS-PES.

It is interesting at this point to also assess the efficiency exhibited by the rovibrational processes involving He atoms as partners, which we have considered here, with other important partners in the early universe environment. For example, vibrational and rotational excitation of HeH^+ due to collisions with electrons was investigated theoretically by Rabadan, Sarpal, and Tennyson[34] and more recently by Ayouz and Kokoouline.[9] When summed over the final rotational states j', the k values for de-excitation from $v = 1$ to $v' = 0$ state varied in the range 10^{-7}–10^{-6} cm^3 molecule^{-1} s^{-1}, considering the temperature range of $0 < T < 500$ K. Similar results were also obtained for de-excitation from the $v = 2$ state to the $v' = 1$ state. There was also a noticeable drop in rate coefficient values, e.g., with k values at 10^{-8}–10^{-7} cm^3 molecule^{-1} s^{-1}, for transitions from the $v = 2$ state to the $v' = 0$ state, when compared to transitions from $v = 2$ to $v' = 1$ in the same temperature range. This simply indicates once more, as we have amply discussed in Sec. IV A for our present results, that the $\Delta v = -2$ transitions are less likely to occur than the $\Delta v = -1$ transitions. In relation with our present calculations, the above values indicate that electrons as collision coolants are able to yield de-excitation rate coefficients for vibrationally "hot" HeH^+, which are about 3 to 4 orders of magnitude larger than in the present case of the He partner.

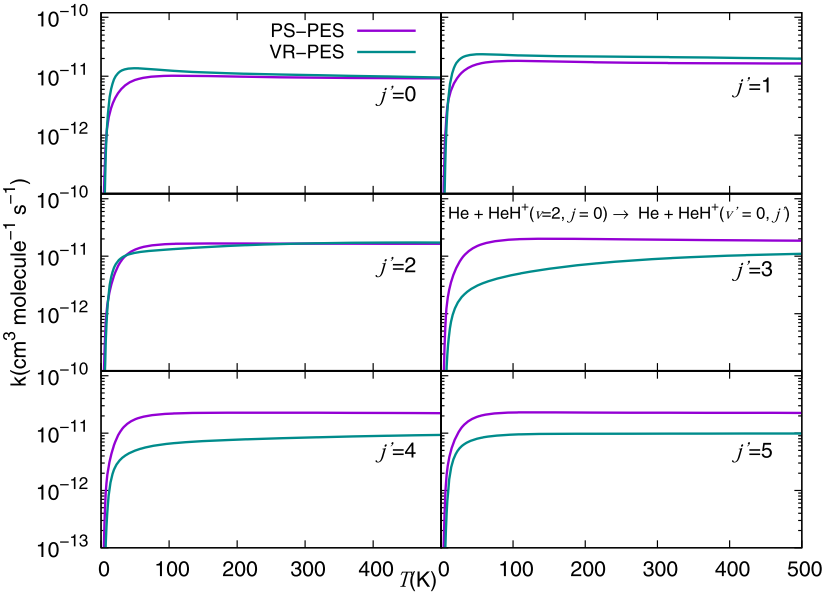


FIG. 16. Comparison of the rate coefficients obtained for transitions from $(v = 2, j = 0)$ to $(v' = 0, j' = 0–5)$ over the same range of temperature discussed in Figs. 14 and 15 using the VR-PES and the PS-PES. See the main text for further details.

Published under an exclusive license by AIP Publishing

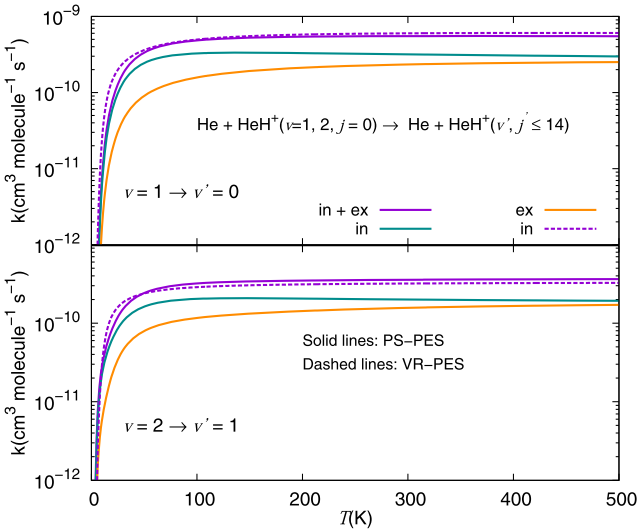


FIG. 17. State-changing rate coefficients involving rovibrational de-excitation paths of HeH^+ from $v = 1$, $j = 0$ to $v' = 0$ and from $v = 2$, $j = 0$ to $v' = 1$. The final channels are summed over all the final j' channels open at each considered energy up to $j' = 14$. The quantum calculations are using the PS-PES and the VR-PES, with the ABC and the ASPIN codes, respectively. The different processes are color-coded in the panels. See the main text for further details.

Although the results of the rate coefficients for the excitation processes can be inferred from the de-excitation rate coefficients via the principle of microscopic reversibility, Ayouz and Kokoouline[9] computed the k values for the $v = 0$ to $v = 1$ transition and found them to be of the order of 10^{-12}–10^{-10} cm^3 molecule^{-1} s^{-1}. In other words, excitation from $v = 0$ to $v = 1$ is less likely to occur than de-excitation from $v = 1$ to $v = 0$ at a given temperature. The work of Ayouz and Kokoouline[9] also pointed out specifically that k for de-excitation in HeH^+-e collisions varied as $1/\sqrt{T}$, while k for excitation varied as $e^{-\Delta\epsilon T}/\sqrt{T}$.

To provide an overall view of the comparative behavior of the final computed rates, we report in the two panels shown in Fig. 17 the results for the two vibrational de-excitation (cooling) processes involving the more efficient $\Delta v = -1$ rovibrational transitions. In the upper panel of Fig. 17, the initial state of the cation is the $v = 1$ state, while in the lower panel of Fig. 17, the initial vibrational state is $v = 2$. We clearly see from the comparison between these data that the results obtained using a purely rovibrationally inelastic scattering code with the new VR-PES yield remarkably similar rate coefficients to those obtained including the proton-exchange process and carrying out the quantum dynamics, inelastic and reactive, with a different scattering code and using the earlier PS-PES discussed in Secs. IV A and IV B: this is a very reassuring result that allows us to further test the reliability of the present calculations. It additionally shows that the rovibrational inelasticity of the He partners by collision with the HeH^+ cation is fairly large and therefore confirms the high efficiency of the present projectiles in causing state-changing processes in HeH^+.

We also see from these computed rate coefficients that, as also expected from the previous discussion in Sec. IV A, the energy-transfer quantities that are produced are essentially the same from both PESs: the overall set of inelastic-plus-exchange channels from the PS-PES and the purely inelastic channels from the VR-PES interaction. In other words, as the proton-exchange channel is included, the quantum dynamics allows for the flux redistribution between reactive and purely inelastic channels while maintaining an overall "energy-transfer" amount that remains the same as when only purely inelastic channels are considered.

Another element of modeling of physical conditions in the ISM environment is the possible information on realistic thermal conditions of the baryons present. The assumption of a local thermodynamic equilibrium (LTE) in different regions of the interstellar medium, in general, is, in fact, expected to hold whenever the population of the excited levels is given by Boltzmann's law. This is likely to occur whenever the rates of spontaneous emission from the internal levels of the polar molecules (in our present case, the rovibrational levels of HeH^+) are smaller than the rate coefficients of collisional de-excitation by the He atoms also present in that ISM region, and hence, the former emission rates can be neglected. This condition implies that the density in the interstellar gas for the interacting partners should be significantly larger than some critical value of that density so that the LTE assumption can be kept as being valid. The definition of such a critical density (e.g., see Refs. 35 and 36) is given as

$$n^i_{\rm crit}(T) = \frac{\sum_{j\neq i} A_{ij}}{\sum_{j\neq i} k_{ij}(T)}. \tag{17}$$

We have considered this sum for the case of $v = 1$ to $v' = 0$, of $v = 2$ to $v' = 1$, and of $v = 2$ to $v' = 0$ transitions, summing over the P and R branches for the rotational levels. We have taken the rate coefficients of the present section by including rotational levels up to $j = 15$ and have employed the Einstein coefficients presented in a very accurate set of calculations in the work of Amaral *et al.*[37]

Between 50 and 500 K, our computed critical densities depended very little on temperature and ranged between 10^{11} and 10^{13} cm^{-3}. These are clearly fairly large values, mainly controlled by the very large radiative emission coefficients, in the numerator of Eq. (17). The two different vibrational cooling processes spanned about two orders of magnitude depending on the considered transition.

The possible values of the baryon densities, n_b, in the environments of the ISM where PNe are present, are estimated to range between about 10^2 cm^{-3} to about 10^6 cm^{-3}. Our computed critical densities for HeH^+ are markedly larger than the above estimates. We, therefore, expect the rovibrational state population of the present cation not to be under LTE conditions since the molecules will radiate well before they can collisionally de-excite. Hence, radiative decay of the internally excited states of the HeH^+ is going to be the dominant channel for energy release in the relevant ISM environments. This is a largely expected result, but the present calculations provide for the first time a quantitative estimate based on realistic calculations.

V. PRESENT CONCLUSIONS

In this study, we discuss in some detail the dynamics of the energy release of an internally excited molecular cation of astrophysical interest, HeH^+, in collision with neutral He atoms. The accurate knowledge of the related state-changing rate coefficients is relevant

Published under an exclusive license by AIP Publishing

for the chemical modeling of the evolutionary kinetics of the cation and for the analysis of its internal state populations under PN conditions. In particular, we have considered the collisional de-excitation ("internal cooling") of rovibrational excited states of the cation when interacting with neutral He atoms at the expected condition of ISM environments.

Our calculations have employed two different, but very similar, potential energy surfaces, which explicitly include the coupling of the motion of the impinging neutral atom with the vibrational and rotational states of the cation. The multi-state collisional dynamics has been treated via the quantum Coupled-Channel (CC) method, which has been implemented both via the *ab inito* PES discussed in our earlier work by Panda and Sathyamurthy[13] and via a newly computed, also *ab initio*, 3D PES discussed in this work in Sec. II and labeled VR-PES throughout this paper.

The quantum dynamics using the PS-PES has been carried out by also including the (non-observable) reactive channel associated with the proton-exchange process and a great variety of inelastic rovibrational processes occurring within the same dynamical event. The multichannel analysis via the newly computed VR-PES has been carried out involving the purely inelastic state-changing channels for the rovibrational processes.

The following results could be evinced from the present calculations:

(i) The final state-to-state cross sections, and the ensuing rate coefficients for T ranging up to 500 K, are seen to be very similar in size and temperature dependence when obtained via the two potential energy surfaces employed in this work.

(ii) When the reactive channels that treat the proton-exchange process are included in the dynamics of the inelastic processes, as done when using the ABC code, the final state-changing events that are given as a sum of both channels turn out to be very close in value to those obtained via the purely inelastic state-changing processes using the ASPIN code and the VR-PES interaction. These findings indicate that the inclusion of the (non-observable) proton-exchange channels subtracts flux to the purely inelastic channels but end up producing the same overall energy-transfer efficiency as obtained from the purely inelastic collisional process.

(iii) In contrast with our earlier findings discussing vibrational cooling of molecular negative ions in collision with He atoms,[38,39] the present results with a cation as a partner for He show that the vibrational and rotational cooling rate coefficients are several orders of magnitude larger than in the case of anionic partners over the same range of T values. Our rovibrational rate coefficients are also of the same order of magnitude as the purely rotationally inelastic rate coefficients of our earlier study (e.g., see Fig. 10 in the work of Gianturco *et al.*[12]).

The present analysis suggests that He atoms are efficient collision partners for the title cation in allowing the flow of its rovibrational internal energy into the ISM environments. The determination of molecular abundance proceeds through a detailed analysis of the molecular emission that arises from regions of very different temperatures and densities. We have quantitatively shown that LTE conditions are not satisfied for this molecular cation, and therefore, a direct and quantitative knowledge of the relevant inelastic rate coefficients can help in setting up more realistic modelings of the chemical evolution in ISM environments. In order to accurately model the observed interstellar spectra and then accurately determine molecular abundances, one must consider the processes of spectral line formation, which, in turn, requires an accurate knowledge of rates for the radiative and collisional excitation of the internal states of the object molecule.

SUPPLEMENTARY MATERIAL

See the supplementary material for the multipolar coefficients for the Legendre expansion of the new VR-PES and the computed transition probabilities and cross sections and rate coefficients that have been obtained by using both the PESs employed in this work.

ACKNOWLEDGMENTS

F.A.G. and R.W. acknowledge the financial support from the Austrian FWF agency through Grant No. P29558-N36. L.G.-S. further acknowledges MINECO (Spain) for funds under Grant No. PGC2018-09644-B-I00; and MCIN/AEI/10.13039/501100011033 (Spain) for funds under Grant. No. PID2020-113147GA-I00.

AUTHOR DECLARATIONS

Conflict of Interest

The authors have no conflicts to disclose.

DATA AVAILABILITY

The data that support the findings of this study are available within the article and in its supplementary material.

REFERENCES

[1] D. Galli and F. Palla, "The dawn of chemistry," Annu. Rev. Astron. Astrophys. **51**, 163 (2013).

[2] S. Lepp, P. C. Stancil, and A. Dalgarno, "Atomic and molecular processes in the early universe," J. Phys. B: At., Mol. Opt. Phys. **35**, R57 (2002).

[3] T. R. Hogness and E. G. Lunn, "The ionization of hydrogen by electron impact as interpreted by positive ray analysis," Phys. Rev. **26**, 44 (1925).

[4] R. Wildt, "Continuous absorption by interstellar molecules," Astron. J. **54**, 139 (1949).

[5] I. Dabrowski and G. Herzberg, "The predicted infrared spectrum of HeH^+ and its possible astrophysical importance," Ann. N. Y. Acad. Sci. **38**, 14 (1977).

[6] R. Güsten, H. Wiesemeyer, D. Neufeld, K. M. Menten, U. U. Graf, K. Jacobs, B. Klein, O. Ricken, C. Risacher, J. Stutzki, and S. Arnouts, "Astrophysical detection of the helium hydride ion HeH," Nature **568**, 357 (2019).

[7] D. A. Neufeld, M. Goto, T. R. Geballe, R. Güsten, K. M. Menten, and H. Wiesemeyer, "Detection of vibrational emissions from the helium hydride ion (HeH^+) in the planetary nebula NGC 7027," Astrophys. J. **894**, 37 (2020).

[8] R. C. Forrey, J. F. Babb, E. D. S. Courtney, R. McArdle, and P. C. Stancil, "Revisiting the formation of HeH^+ in the planetary nebula NGC 7027," **898**, 86 Astrophys. J. (2020).

[9] M. Ayouz and V. Kokoouline, "Cross sections and rate coefficients for rovibrational excitation of HeH^+ isotopologues by electron impact," Atoms **7**, 67 (2019).

[10] J. R. Hamilton, A. Faure, and J. Tennyson, "Electron-impact excitation of diatomic hydride cations—I. HeH^+, CH^+, ArH^+," Mon. Not. R. Astron. Soc. **455**, 3281 (2016).

Published under an exclusive license by AIP Publishing

[11]B. Desrousseaux and F. Lique, "Collisional energy transfer in the HeH^+–H reactive system," J. Chem. Phys. **152**, 074303 (2020).
[12]F. A. Gianturco, K. Giri, L. González-Sánchez, E. Yurtsever, N. Sathyamurthy, and R. Wester, "Energy-transfer quantum dynamics of HeH^+ with He atoms: Rotationally inelastic cross sections and rate coefficients," J. Chem. Phys. **154**, 054311 (2021).
[13]A. N. Panda and N. Sathyamurthy, "Bound and quasibound states of He_2H^+ and He_2D^+," J. Phys. Chem. A **107**, 7125 (2003).
[14]J.-J. Liang, C.-L. Yang, L.-Z. Wang, and Q.-G. Zhang, "A new analytical potential energy surface for the singlet state of He_2H^+," J. Chem. Phys. **136**, 094307 (2012).
[15]S. Bhattacharya and A. N. Panda, "Time-dependent quantum dynamics of the He + H^+He reaction," J. Phys. B: At., Mol. Opt. Phys. **42**, 085201 (2009).
[16]W. Xu and P. Zhang, "Accurate study on the quantum dynamics of the He + HeH^+ ($X^1\ \Sigma^+$) reaction on A new ab initio potential energy surface for the lowest $1^1A'$ electronic singlet state," J. Phys. Chem. A **117**, 1406 (2013).
[17]D. Wu, M. Guo, Y. Wang, S. Yin, Z. Sun, and M. R. Hoffmann, "Coriolis coupling effect of state-to-state quantum dynamics for He + HeH^+," Theor. Chem. Acc. **133**, 1552 (2014).
[18]H.-J. Werner, P. J. Knowles, G. Knizia, F. R. Manby, and M. Schütz, "Molpro: A general-purpose quantum chemistry program package," Wiley Interdiscip. Rev.: Comput. Mol. Sci. **2**, 242–253 (2012).
[19]H.-J. Werner, P. J. Knowles, G. Knizia, F. R. Manby, M. Schütz *et al.*, MOLPRO, version 2019.2, a package of *ab initio* programs, 2019, see https://www.molpro.net.
[20]C. Hampel, K. A. Peterson, and H.-J. Werner, "A comparison of the efficiency and accuracy of the quadratic configuration interaction (QCISD), coupled cluster (CCSD), and Brueckner coupled cluster (BCCD) methods," Chem. Phys. Lett. **190**, 1–12 (1992).
[21]M. J. O. Deegan and P. J. Knowles, "Perturbative corrections to account for triple excitations in closed and open shell coupled cluster theories," Chem. Phys. Lett. **227**, 321–326 (1994).
[22]D. E. Woon and T. H. Dunning, Jr., "Gaussian basis sets for use in correlated molecular calculations. III. The atoms aluminum through argon," J. Chem. Phys. **98**, 1358 (1993).
[23]D. E. Woon and T. H. Dunning, Jr., "Gaussian basis sets for use in correlated molecular calculations. IV. Calculation of static electrical response properties," J. Chem. Phys. **100**, 2975 (1994).
[24]R. J. Le Roy, "LEVEL: A computer program for solving the radial Schrödinger equation for bound and quasibound levels," J. Quant. Spectrosc. Radiat. Transfer **186**, 167 (2017).
[25]H. J. Werner, B. Follmeg, and M. H. Alexander, "Adiabatic and diabatic potential energy surfaces for collisions of CN ($X^2\Sigma^+$, $A^2\pi$) with He," J. Chem. Phys. **89**, 3139 (1988).
[26]C. Balança and F. Dayou, "Ro-vibrational excitation of SiO by collision with helium at high temperature," Mon. Not. R. Astron. Soc. **469**, 1673 (2017).
[27]D. López-Durán, E. Bodo, and F. A. Gianturco, "ASPIN: An all spin scattering code for atom-molecule rovibrationally inelastic cross sections," Comput. Phys. Commun. **179**, 821 (2008).
[28]A. M. Arthurs and A. Dalgarno, "The theory of scattering by a rigid rotator," Proc. R. Soc. London, Ser. A **256**, 540 (1960).
[29]D. E. Manolopoulos, "An improved log derivative method for inelastic scattering," J. Chem. Phys. **85**, 6425 (1986).
[30]R. Martinazzo, E. Bodo, and F. A. Gianturco, "A modified variable-phase algorithm for multichannel scattering with long-range potentials," Comput. Phys. Commun. **151**, 187 (2003).
[31]B. P. Mant, F. A. Gianturco, L. González-Sánchez, E. Yurtsever, and R. Wester, "Rotationally inelastic processes of C_2^- ($^2\sigma_g^+$) colliding with He (^1S) at low-temperatures: *Ab Initio* interaction potential, state-changing rates and kinetic modelling," J. Phys. B: At., Mol. Opt. Phys. **53**, 025201 (2020).
[32]D. Skouteris, J. F. Castillo, and D. E. Manolopoulos, "ABC: A quantum reactive scattering program," Comput. Phys. Commun. **133**, 128 (2000).
[33]I. W. M. Smith, "Relaxations in collisions of vibrationally excited molecules with potentially reactive atoms," Acc. Chem. Res. **9**, 161 (1976).
[34]I. Rabadán, B. K. Sarpal, and J. Tennyson, "Calculated rotational and vibrational excitation rates for electron—HeH^+ collisions," Mon. Not. R. Astron. Soc. **299**, 171 (1998).
[35]M. Lara-Moreno, T. Stoecklin, and P. Halvick, "Rotational transitions of C_3N^- induced by collision with H_2," Mon. Not. R. Astron. Soc. **486**, 414 (2019).
[36]O. Yazidi, D. Ben Abdallah, and F. Lique, "Revised study of the collisional excitation of HCO^+ by $H_2(j = 0)$," Mon. Not. R. Astron. Soc. **441**, 664 (2014).
[37]P. H. R. Amaral, L. G. Diniz, K. A. Jones, M. Stanke, A. Alijah, L. Adamowicz, and J. R. Mohallem, "Benchmark rovibrational linelists and Einstein A-coefficients for primordial molecules and isotopologues," Astrophys. J. **878**, 95 (2019).
[38]B. P. Mant, F. A. Gianturco, R. Wester, E. Yurtsever, and L. González-Sánchez, "Ro-vibrational quenching of C_2^- anions in collisions with He, Ne and Ar atoms," Phys. Rev. A **102**, 062810 (2020).
[39]B. Mant, E. Yurtsever, L. González-Sánchez, R. Wester, and F. A. Gianturco, "Vibrational quenching of CN^- in collisions with He and Ar," J. Chem. Phys. **154**, 084305 (2021).

Published under an exclusive license by AIP Publishing